Push-Pull Design of Bis(tridentate) Ruthenium(II) Polypyridine Chromophores as Deep Red Light Emitters in Light-Emitting Electrochemical Cells

Aaron Breivogel,[a] Myeongjin Park,[b] Donggu Lee,[b] Stefanie Klassen,[c] Angelika Kühnle,[c] Changhee Lee,[b] Kookheon Char,[d] and Katja Heinze*[a]

Dedicated to Professor Rudolf Zentel on the occasion of his 60th birthday

Light-emitting electrochemical cells (LECs) with a simple device structure were prepared by using heteroleptic bis(tridentate) ruthenium(II) complexes [**1**](PF$_6$)$_2$–[**3**](PF$_6$)$_2$ as emitters. The push-pull substitution shifts the emission energy to low energy, into the NIR region. The devices emit deep red light up to a maximum emission wavelength of 755 nm [CIE (International Commission on Illumination) coordinates: x = 0.731, y = 0.269 for [**3**](PF$_6$)$_2$], which, to the best of our knowledge, is the lowest emission energy for LECs containing bis(tridentate) ruthenium(II) complexes. A device structure of ITO/PEDOT:PSS/ruthenium(II) complex/Ag was used, and the thickness of the emitting layer was measured by AFM [ITO: indium tin oxide, PEDOT: poly(3,4-ethylenedioxythiophene), PSS: poly(styrenesulfonate), AFM: atomic force microscopy]. To enhance the external quantum efficiency (EQE), cells were fabricated with and without poly(methyl methacrylate) (PMMA) as additive in the emitting layer.

Introduction

Light-emitting electrochemical cells (LECs) provide a low-cost alternative to conventional organic light emitting devices (OLEDs) due to their simple device structures and solution processability. LECs feature an ionic emitting layer that enables low turn-on and driving voltages, as well as independence of the work function of electrode materials.[1–6] LECs introduced in 1995 by Pei contained organic polymers as emitters.[7,8] While for all-organic emitters spin statistics predicts a maximum internal quantum efficiency of 25%, transition metal complexes have a theoretical limit of 100%, because in the latter both singlet and triplet excitons can lead to light emission.[9–12] The first LEC with an ionic transition metal complex was reported in 1996 by Lee employing a [Ru(phen)$_3$]$^{2+}$ derivative as emitter (phen: 1,10-phenanthroline).[13] The use of ruthenium(II) complexes as emitters is reasonable because of their outstanding photophysical and electrochemical properties combined with their high thermal and chemical stabilities.[14] So far [Ru(bpy)$_3$]$^{2+}$ (bpy: 2,2′-bipyridine) and its analogues are the most studied ruthenium(II) polypyridine complexes because they have high ^{3}MLCT (MLCT: metal-to-ligand charge transfer) excited state lifetimes ($\tau \approx 1$ µs) and luminescence quantum yields ($\Phi \approx 10$%) at room temperature in solution.[14–16] [Ru(bpy)$_3$]$^{2+}$ and its derivatives have already been used in LECs showing high external quantum efficiencies (EQEs) of up to 6.4%.[17–20]

However, [Ru(bpy)$_3$]$^{2+}$ is chiral (Δ, Λ), and unsymmetrical substitution of bpy ligands leads to the formation of stereoisomers, which complicates synthetic procedures.[21,22] The formation of stereoisomers can be avoided by using tridentate, meridional coordinating ligands. For instance achiral [Ru(tpy)$_2$]$^{2+}$ (tpy: 2,2′;6′,2′′-terpyridine) gives rise to only a single isomer even in the case of unsymmetrical substitution of the tpy 4′-positions.[23] Additionally, the tridentate coordination provides a higher photostability and

[a] Institute of Inorganic Chemistry and Analytical Chemistry, Johannes Gutenberg University of Mainz, Duesbergweg 10-14, 55128 Mainz, Germany
E-mail: katja.heinze@uni-mainz.de
http://www.ak-heinze.chemie.uni-mainz.de/
[b] Department of Electrical and Computer Engineering, Inter-University Semiconductor Research Center, Seoul National University, 1 Gwanak-ro, Gwanak-gu, Seoul 151-744, Korea
[c] Institute of Physical Chemistry, Johannes Gutenberg University of Mainz, Duesbergweg 10-14, 55099 Mainz, Germany
[d] The National Creative Research Initiative Center for Intelligent Hybrids, The WCU Program on Chemical Convergence for Energy and Environment, School of Chemical and Biological Engineering, Seoul National University, 1 Gwanak-ro, Gwanak-gu, Seoul, 151-744, Korea

Wiley Online Library

chemical stability relative to the bidentate mode.[24,25] This should prevent thermal and photoinduced ligand exchange, favoring longevity of luminescent and solar cell devices.[26–29] Degradation products due to ligand loss have been identified in LECs with $[Ru(bpy)_3]^{2+}$ complexes, namely bis(aqua)complex $[Ru(bpy)_2(H_2O)_2]^{2+}$ and oxido-bridged dimer $[\{Ru(bpy)_2(H_2O)\}_2O]^{4+}$, which have been formed by photoaquation in the presence of water.[6,30–32] A better stabilization towards (photo) ligand substitution might be achieved by using tridentate ligands.

Unfortunately, excited state features of $[Ru(tpy)_2]^{2+}$ in solution are very unfavorable ($\tau \approx 0.1$–0.2 ns, $\Phi \leq 0.0005\%$) because of rapid radiationless deactivation of the radiative ^{3}MLCT states via thermally accessible ^{3}MC states (MC: metal-centered; Figure 1).[33,34] Increased excited state lifetimes τ and quantum yields Φ have been obtained by structurally modifying $[Ru(tpy)_2]^{2+}$ in order to increase the energy difference between the ^{3}MLCT and ^{3}MC states and hence to avoid radiationless deactivation via the latter states. Push-pull substitution like that in $[(EtOOC-tpy)-Ru(tpy-NH_2)]^{2+}$ ($[\mathbf{1}](PF_6)_2$, Figure 2) is favorable, as the electron-withdrawing ester group lowers the energy of the ^{3}MLCT state while the electron-donating amino group increases the energy of the ^{3}MC state, thus reducing radiationless deactivation via the latter state and enhancing the excited state lifetime and luminescence quantum yield significantly ($\tau = 34$ ns, $\Phi = 0.18\%$).[23,35–37] Another strategy employs a strong ligand field to increase the energy difference between the ^{3}MLCT and ^{3}MC states. This can be achieved by N–Ru–N bite angles of 90° as in an ideal octahedron allowing for an optimal overlap of ruthenium and nitrogen orbitals. The N–Ru–N bite angle of tpy is 79° because its five-membered chelate rings result in a suboptimal orbital overlap.[38] Hammarström et al. designed a complex $\{[Ru(dqp)_2]^{2+}$; dpq: 2,6-di(quinolin-8-yl)pyridine} with six-membered chelate rings and 90° bite angles featuring high room-temperature lifetime and quantum yield in solution ($\tau = 3.0$ µs, $\Phi = 2\%$).[39,40] The substituted complex $[Ru(dpq-COOEt)_2]^{2+}$ with ester substituents on the 4′-positions reaches even higher values ($\tau = 5.5$ µs, $\Phi = 7\%$).[41] Ruben et al. incorporated carbonyl bridges between the pyridine rings of $[Ru(tpy)_2]^{2+}$ and thus obtained six-membered chelate rings and 90° bite angles leading to high ^{3}MLCT lifetimes and, to the best of our knowledge, to the highest re-

ported quantum yield of bis(tridentate) ruthenium(II) complexes ($\tau = 3.3$ µs, $\Phi = 30\%$).[42] Bis(tridentate) ruthenium(II) complexes have been incorporated in LECs, but until now only complexes with small bite angles (ca. 79°) and hence low solution luminescence quantum yields have been utilized, leading to low EQEs ($\leq 0.1\%$) of the devices.[43–45]
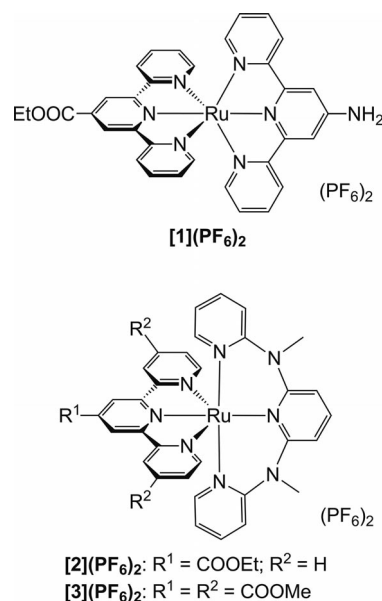
Figure 2. Bis(tridentate) ruthenium(II) oligopyridine complexes $[\mathbf{1}](PF_6)_2$–$[\mathbf{3}](PF_6)_2$.

In this paper, we incorporate bis(tridentate) ruthenium(II) complexes $[\mathbf{1}](PF_6)_2$–$[\mathbf{3}](PF_6)_2$ as low-energy emitters in LECs (Figure 2). $[\mathbf{1}](PF_6)_2$–$[\mathbf{3}](PF_6)_2$ are photostable and chemically stable as a result of their tridentate coordination mode; they feature a sophisticated push-pull substitution with high directionality due to electron-withdrawing ester and electron-donating amino groups.[35–37,46–48] The push-pull substitution lowers the HOMO–LUMO gap (and hence increases the energy difference between the ^{3}MLCT and ^{3}MC states) and leads to emission in the red spectral region ($\lambda_{em} = 729$–744 nm, Table 1).[35,36,46,47] Red light and NIR emission are particularly favorable for noninvasive bioimaging, telecommunication, night-vision-readable displays, downconversion and triplet–triplet annihilation upconversion.[1,2,49–57] However, according to the energy gap law, low-energy emission is correlated to low luminescence quantum yields and short luminescence lifetimes due to effective radiationless deactivation into the ground state.[58–60] In spite of their low emission energy, complexes $[\mathbf{1}](PF_6)_2$–$[\mathbf{3}](PF_6)_2$ possess comparably high luminescence lifetimes and quantum yields at room temperature in solution ($\tau = 34$, 722, and 841 ns; $\Phi = 0.18$, 0.45, and 1.1%, Table 1). While complex $[\mathbf{1}](PF_6)_2$ consists of two tpy ligands with 79° N–Ru–N bite angles, complexes $[\mathbf{2}](PF_6)_2$ and $[\mathbf{3}](PF_6)_2$ consist of a tpy ligand and a ddpd ligand (ddpd: N,N′-dimethyl-N,N′-dipyridin-2-ylpyridine-2,6-diamine).[35,46,47] The larger bite angle (88°) of the latter ligand favors the
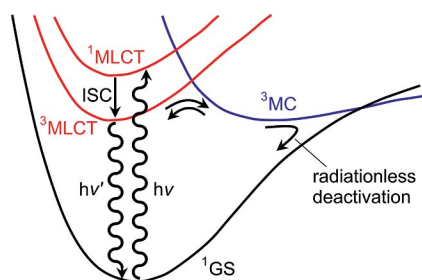
Figure 1. Jablonski diagram of ruthenium(II) polypyridine complexes (GS: ground state, MLCT: metal-to-ligand charge transfer, ISC: intersystem crossing, MC: metal centered).

high luminescence lifetimes and quantum yields of [**2**]-$(PF_6)_2$ and [**3**]$(PF_6)_2$ (Φ = 0.45 and 1.1%, Table 1) and their choice as red light to NIR emitters in LECs.

Table 1. Electrochemical and photophysical properties of complexes [**1**]$(PF_6)_2$–[**3**]$(PF_6)_2$.[35–37,46]

	[**1**]$(PF_6)_2$	[**2**]$(PF_6)_2$	[**3**]$(PF_6)_2$
$E_{1/2}^{ox}$ /V[a]	+0.68	+0.81	+0.92
$E_{1/2}^{red}$ /V[a]	–1.54,	–1.47,	–1.25[b],
	–1.99	–2.09[b]	–1.70[b]
λ_{abs} /nm (ε/M^{-1} cm^{-1})[c]	502 (19080)	517 (7500)	539 (6360),
			475 (5060)
$\lambda_{em,295\,K}$ /nm[c]	734	729	744
$\Phi_{295\,K}$ /%[c]	0.18	0.45	1.1
$\tau_{295\,K}$ /ns	34[c]	722[d]	841[d]

[a] In 0.1 M [nBu_4N][PF_6] in CH_3CN vs. Fc/Fc$^+$. [b] Irreversible, E_p given. [c] In CH_3CN. [d] In PrCN.

Results and Discussion

The electrochemical and photophysical properties of complexes [**1**]$(PF_6)_2$–[**3**]$(PF_6)_2$ have been described previously and are summarized in Table 1.[35–37,46] The oxidation potential, $E_{1/2}^{ox}$, follows the order [**1**]$(PF_6)_2$ < [**2**]$(PF_6)_2$ < [**3**]$(PF_6)_2$ (Table 1). [**1**]$(PF_6)_2$ is oxidized at the lowest potential because of the electron-donating effect of the NH_2 substituent. [**3**]$(PF_6)_2$ is oxidized at the highest potential because of the electron-withdrawing effect of the three ester groups.[46] The first reduction potential, $E_{1/2}^{red}$, follows the same order [**1**]$(PF_6)_2$ < [**2**]$(PF_6)_2$ < [**3**]$(PF_6)_2$ (Table 1) for the same reasons as those for the trend in $E_{1/2}^{ox}$. The oxidation of [**1**]$(PF_6)_2$–[**3**]$(PF_6)_2$ is reversible on the time scale of electrochemical experiments, while reduction is only reversible for [**1**]$(PF_6)_2$ and [**2**]$(PF_6)_2$ on this time scale. The reduction of [**3**]$(PF_6)_2$ seems to be only quasireversible.[35,36,46] Thus, for all complexes sufficient reversibility in oxidation and reduction processes is given for the application in LECs.

HOMO and LUMO energies of emitting compounds [**1**]$(PF_6)_2$–[**3**]$(PF_6)_2$ were estimated from electrochemical redox potentials (Table 1) and are depicted in Figure 3.[61] The parent [$Ru(tpy)_2$]$^{2+}$ complex has a HOMO–LUMO energy gap of ΔE = 2.59 eV with E_{HOMO} = –6.00 eV and E_{LUMO} = –3.41 eV.[23] The effect of donor–acceptor substitution in [**1**]$(PF_6)_2$ can be clearly seen as the electron-withdrawing ester group lowers the LUMO energy (E_{LUMO} = –3.54 eV) while the electron-donating amino group raises the HOMO energy (E_{HOMO} = –5.76 eV) resulting in a smaller ΔE = 2.22 eV compared to that of [$Ru(tpy)_2$]$^{2+}$. [**2**]$(PF_6)_2$ and [**3**]$(PF_6)_2$ have lower HOMO and LUMO energies than [**1**]$(PF_6)_2$ because of the strong electron-donating effect of the primary amino group present in [**1**]-$(PF_6)_2$.[35–37,46] [**3**]$(PF_6)_2$ has even lower HOMO and LUMO energies than [**2**]$(PF_6)_2$, which results from the electron-withdrawing character of the additional ester groups on the tpy ligand. The push-pull effect is most pronounced in [**3**]$(PF_6)_2$, leading to the smallest HOMO–LUMO energy gap in this series (E_{HOMO} = –6.00 eV, E_{LUMO} = –3.83 eV,

ΔE = 2.17 eV). HOMO and LUMO energies were also obtained by DFT calculations and are summarized in Figure 3.

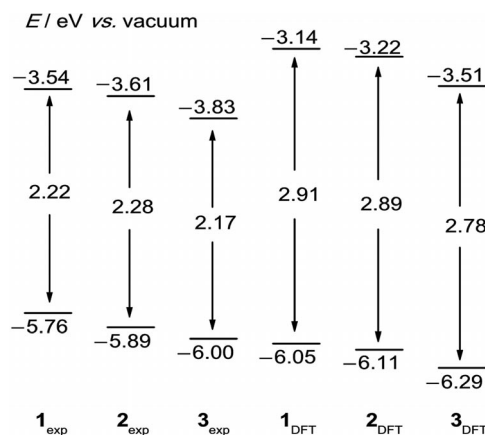Figure 3. HOMO and LUMO levels of complexes [**1**]$(PF_6)_2$–[**3**]$(PF_6)_2$ from experimentally determined redox potentials in CH_3CN[35,46] and from DFT calculations (B3LYP/LANL2DZ, IEFPCM, CH_3CN).

HOMO energies calculated by DFT (B3LYP/LANL2DZ, IEFPCM, CH_3CN) are lower (0.2–0.3 eV) and LUMO energies are higher (0.3–0.4 eV) than values obtained from electrochemical data. Nevertheless, the trend of the HOMO and LUMO energies (E_{HOMO} and E_{LUMO}) is correctly reproduced: [**1**]$^{2+}$ > [**2**]$^{2+}$ > [**3**]$^{2+}$.

The injection of electrons and holes from opposite electrodes leads to the formation of radical species. Electron capture and loss both occur on the doubly charged ruthenium complex cation. Reduction is located at the ester-substituted tpy ligands, while oxidation is essentially confined to the ruthenium center.[35,46–48] Spin densities calculated by DFT are exemplarily depicted for complex [**3**]$^{2+}$ in its reduced and oxidized forms ([**3**]$^+$ and [**3**]$^{3+}$; Figures 4a and 4b). The plot illustrates the location of reduction and oxidation processes in [**3**]$^{2+}$. Electron transfer from [**3**]$^+$ to [**3**]$^{3+}$ leads to one ^{1,3}MLCT excited state species ^{1,3}[**3**]$^{2+}$ and [**3**]$^{2+}$ in the ground state.[62] The excited ^{1}MLCT state undergoes efficient ISC to the ^{3}MLCT state (Figure 1).[16] Finally, the ^{3}MLCT state emits light upon returning to the singlet ground state [**3**]$^{2+}$ (Figure 1). The spin density of ^{3}[**3**]$^{2+}$ is located on both the ruthenium center and the ester-substituted tpy ligand (Figure 4c), which is in accord with a ruthenium(III) center and a one-electron-reduced tpy ligand.

LECs incorporating [**1**]$(PF_6)_2$–[**3**]$(PF_6)_2$ were built with a configuration of ITO/PEDOT:PSS/ruthenium(II) complex/ Ag [Figure 5; ITO: indium tin oxide; PEDOT: poly(3,4-ethylenedioxythiophene); PSS: poly(styrenesulfonate)]. PEDOT:PSS was found to increase reproducibility[45] and shows a HOMO energy level of E_{HOMO} = –5.1 eV.[63] Ag was used as cathode material because it greatly improves lifetimes of LECs compared to other electrode materials like Al.[20] Cells were fabricated with and without 20% (w/w) PMMA in the emitting layer [PMMA: poly(methyl methacrylate)]. PMMA acts as insulator, improves the film
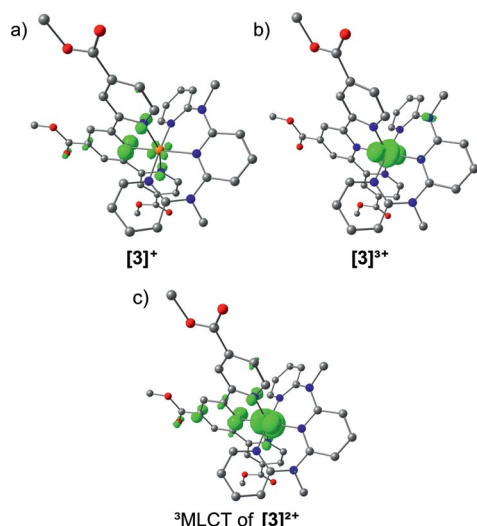
Figure 4. Spin densities of (a) one-electron-reduced complex $[\mathbf{3}]^+$, (b) one-electron-oxidized complex $[\mathbf{3}]^{3+}$ and (c) the lowest excited triplet species ^{3}MLCT of $[\mathbf{3}]^{2+}$ in CH$_3$CN calculated by DFT (B3LYP/LANL2DZ, IEFPCM, contour value 0.01 a. u.). Hydrogen atoms are omitted.

Figure 6. AFM image taken in intermittent contact mode of a scratched PEDOT:PSS/$[\mathbf{1}]$(PF$_6$)$_2$ with PMMA layer. (a) Topographical height scan with indicated cross section. (b) Height profile along the indicated cross section.

quality, and increases the distance between ruthenium(II) complexes to avoid self-quenching processes to enhance the EQE and to prolong device lifetimes.[18,20,44,45,64] The PEDOT:PSS and ruthenium(II) complex layers were spin-coated onto an ITO substrate. The Ag cathode was deposited in vacuo by thermal evaporation. The thicknesses of the PEDOT:PSS and the ruthenium complex:PMMA layers were determined by AFM measurements after scratching the layer with a razor (AFM: atomic force microscopy). The thicknesses are 45 ± 5 nm (PEDOT:PSS), 229 ± 19 nm (total thickness of PEDOT:PSS and ruthenium complex without PMMA), and 237 ± 23 nm (total thickness of PEDOT:PSS and ruthenium complex with PMMA). Figure 6 shows a representative AFM image of the scratched LEC with $[\mathbf{1}]$(PF$_6$)$_2$ and PMMA. AFM images for all scratched LECs are depicted in the Supporting Information (Figure S1).
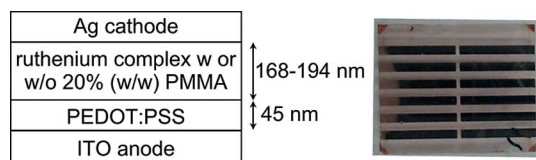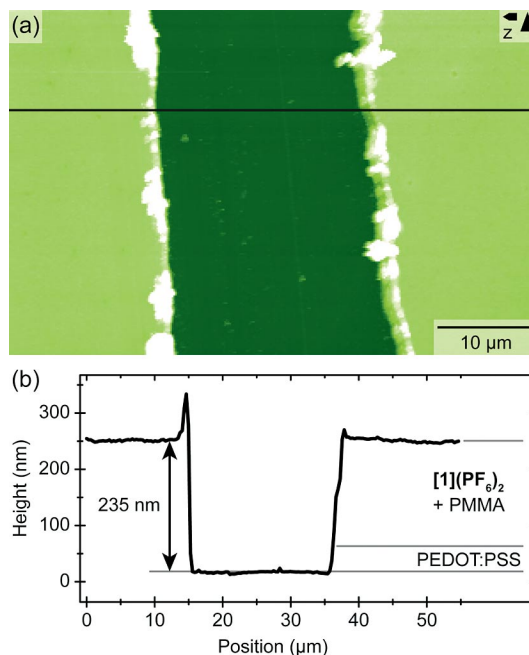

Figure 5. General device structure of the LECs and photograph of the LEC with $[\mathbf{1}]$(PF$_6$)$_2$ without PMMA.

A voltage of 3 V was applied to each cell for at least 10 min. The LEC incorporating complex $[\mathbf{2}]$(PF$_6$)$_2$ (without PMMA) shows red light emission. The other cells did not emit under these conditions. For these cells, a higher voltage on a new pixel was applied in steps of 0.5–1 V until emission was observed. LEC characteristics are summarized in Table 2. The reported voltage is the minimum voltage for which emission is observed, and all other data refer to this voltage. Cells with $[\mathbf{1}]$(PF$_6$)$_2$ without PMMA do not emit

up to a voltage of 6 V. When PMMA is present, the LEC with $[\mathbf{1}]$(PF$_6$)$_2$ emits with a turn on voltage of 4 V. The driving voltages are generally a few volts higher for cells with PMMA, which is consistent with the insulating character of PMMA.[20] Emission wavelengths of the devices are fully comparable to the emissions in solution and differ only by $\Delta E = \pm 0.02$ eV (Tables 1 and 2, Figures S2 and S3). $[\mathbf{3}]$(PF$_6$)$_2$ features a slightly redshifted electroluminescence in LECs in the absence of PMMA (Figure S4, Tables 1 and 2). Figure 7a exemplarily depicts the emission spectra of $[\mathbf{2}]$(PF$_6$)$_2$ in CH$_3$CN and in LECs with and without PMMA.

The longest emission wavelength maximum ($\lambda_{em,max} = 755$ nm) was obtained for the LEC with $[\mathbf{3}]$(PF$_6$)$_2$ without PMMA at an applied voltage of 4 V. To the best of our knowledge, this is the longest emission wavelength of a LEC with a mononuclear bis(tridentate) ruthenium(II) complex. The CIE (International Commission on Illumination) coordinates[65] of the emitted light are given in Table 2 and in all cases correspond to deep red light at the edge of the CIE chromaticity diagram. Light intensity, current density, and EQE curves are plotted against time (Supporting Information, Figures S4–S7). Exemplarily, Figure 7b shows the EQE-intensity-current density vs. time plots for the LEC with $[\mathbf{2}]$(PF$_6$)$_2$ without PMMA at an applied voltage of 3 V. All values increase at initial stages until they reach a maximum after a few minutes. Then they slowly decrease as typically observed for this kind of LECs.[44,45] Maximum light emission occurs after $t_{em,max} = 2$–14 min. Devices with PMMA should have a higher $t_{em,max}$ than devices without PMMA, because PMMA hinders ion migration and forma-

Table 2. LEC device characteristics for complexes [**1**](PF$_6$)$_2$–[**3**](PF$_6$)$_2$.

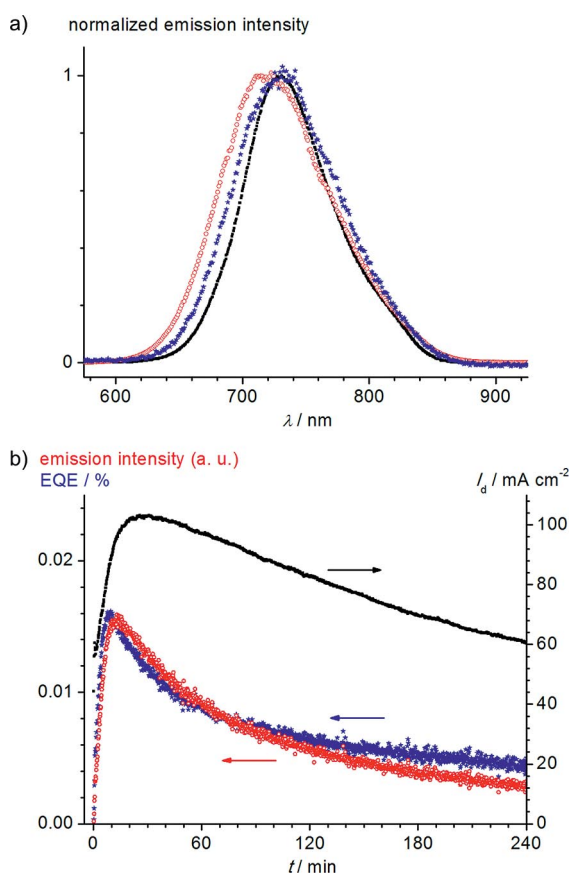|	[**1**](PF$_6$)$_2$ without PMMA	with PMMA[a]	[**2**](PF$_6$)$_2$ without PMMA	with PMMA[a]	[**3**](PF$_6$)$_2$ without PMMA	with PMMA[a]
Height of emitting layer /nm	182 ± 16	190 ± 12	168 ± 33	191 ± 31	193 ± 27	194 ± 12
U /V	–	4	3	6	4	5
$\lambda_{em,max,LEC}$ /nm	–	733$^{(6V)}$	731	722	755	745
$\lambda_{em,max,acetonitrile}$ /nm	734	734	729	729	744	744
$t_{em,max}$ /min	–	ca. 11–14	13	2	9	4
L_{max} /cd m^{-2}	–	0.32	1.81	3.36	0.75	0.64
$t_{current,max}$ /min	–	13	31	3	8	8
$I_{d,max}$ /mA cm^{-2}	–	313	103	518	213	231
EQE$_{max}$ /%	–	0.001	0.016	0.028	0.007	0.013
$t_{EQE,max}$ /min	–	14–15	10	1	9	1
CIE coordinates (x, y)	–	0.709, 0.291	0.725, 0.275	0.717, 0.283	0.731, 0.269	0.729; 0.271

[a] 20 % (w/w).

Figure 7. (a) Normalized emission spectra of [**2**](PF$_6$)$_2$ (black squares: CH$_3$CN solution; red hollow circles: LEC with PMMA, 6 V; blue stars: LEC without PMMA, 3 V). (b) Current density (black squares), emission intensity (red hollow circles), and EQE (blue stars) as a function of time in the LEC with [**2**](PF$_6$)$_2$ without PMMA at an applied voltage of 3 V.

device was a Lambertian source and a calibrated Si photodiode was placed at an angle normal to the device surface.[66,67]

$$L = \frac{K_m \cdot I_{photodiode} \cdot R^2}{A_{LEC} \cdot A_{photodiode}} \frac{\int_{360nm}^{830nm} V(\lambda) \frac{S_{emission}(\lambda)}{S_{responsivity}(\lambda)} d\lambda}{\int_{360nm}^{830nm} S_{emission}(\lambda) d\lambda}$$

(1)

where K_m = 683 lm W^{-1} at 555 nm, I: current, R: distance between LEC and photodiode, A_{LEC}: area of the limiting aperture, $A_{photodiode}$: area of the photodiode, $V(\lambda)$: photopic response curve, $S_{emission}(\lambda)$: emission spectrum, $S_{responsivity}(\lambda)$: responsivity of the Si photodiode, λ: wavelength).

The highest luminance is L = 3.4 cd m^{-2} for the LEC with [**2**](PF$_6$)$_2$ with PMMA at an applied voltage of 6 V. The smaller luminance of LECs with [**1**](PF$_6$)$_2$ (L = 0.3 cd m^{-2}) is likely due to the lower luminescence quantum yield of [**1**](PF$_6$)$_2$ in solution (Table 2). The lower luminance of [**3**](PF$_6$)$_2$ ($L \approx 0.7$ cd m^{-2}) might be due to the small overlap of its NIR emission ($\lambda_{em} \approx 750$ nm) with the human eye response curve (Figure S8). The current density reaches its maximum after $t_{current,max}$ = 3–31 min. For LECs with complex [**3**](PF$_6$)$_2$ there is no clear dependency of $t_{current,max}$ on the voltage or the presence of PMMA. In contrast, $t_{current,max}$ values in LECs with [**2**](PF$_6$)$_2$ are smaller at high voltages (6 V, 3 min) and larger at lower voltages (3 V, 31 min), which confirms that ion migration is faster at higher voltages.[6] Current densities are in the range I_d = 103–518 mA cm^{-2}, which is consistent with previously reported LECs with a bis(terpyridine)ruthenium(II) complex (ca. 200–300 mA cm^{-2}).[44] As expected, current densities are high for high applied voltages (Table 2). EQE values are 0.001–0.028 %. The highest EQE value (0.028 %) is obtained for the LEC with [**2**](PF$_6$)$_2$ with PMMA. LECs containing [**1**](PF$_6$)$_2$ only lead to a small EQE (0.001 %), which is probably caused by the smaller solution quantum yield of [**1**](PF$_6$)$_2$ relative to those of [**2**](PF$_6$)$_2$ and [**3**](PF$_6$)$_2$ (Table 1). The maximum EQE of the LEC with [**3**](PF$_6$)$_2$ (0.013 %) is less than the EQE for the LEC with [**2**](PF$_6$)$_2$ (0.028 %), which is in contrast to the relative emission quan-

tion of electric double layers. However, a smaller $t_{em,max}$ value is measured for devices with PMMA than for those without PMMA (see LECs with [**2**](PF$_6$)$_2$ and [**3**](PF$_6$)$_2$, Table 2). The higher voltages applied for devices with PMMA to compensate the insulating behavior of PMMA might be responsible for this observation.[6] Luminances L were calculated with Equation (1), which assumes that the

tum yields (Table 1 and Table 2). Possibly this observation can be explained by the redshifted emission of [**3**]$(PF_6)_2$ (λ = 745–755 nm) within the LEC compared to its emission in solution (λ = 744 nm, Figure S5, Table 1 and Table 2). The low-energy emissive state might be prone to enhanced radiationless deactivation according to the energy gap law.[58–60] Interestingly, [**2**]$(PF_6)_2$ shows no redshifted emission in the LECs (Figure 7a, Table 1 and Table 2).

For OLEDs, saturation and quenching effects like triplet–triplet annihilation resulting from high luminescence lifetimes and high current densities can lead to decreasing EQEs.[68] Typically, luminescent emitters are doped into host matrices like PMMA or CBP in order to enhance the EQE [CBP: 4,4′-bis(9-carbazolyl)-2,2′-biphenyl]. For instance, fac-Ir(ppy)$_3$ (ppy: 2-phenylpyridine) features lifetimes of 1.4 µs (less than 0.1 w/w% in PMMA) to 630 ns (8 w/w% in CBP), which is regarded sufficiently short to avoid saturation and quenching effects up to a current density of I_d = 1000 mA cm^{-2}.[69,70] Saturation thresholds for the current density also depend on the concentration of the dopant. For PtOEP (PtOEP: 2,3,7,8,12,13,17,18-octaethylporphyrine platinum) with a phosphorescence lifetime of τ ≈ 30 µs, the critical current density rises from I_d = 40 (1 w/w% in CBP) to 800 mA cm^{-2} (16 w/w% in CBP).[71] For neat films of fac-Ir(ppy)$_3$ the EQE drops to 0.8% with a concomitant drop in phosphorescence lifetime to τ ≈ 100 ns relative to doped devices.[72] This drop is caused by self-quenching due to Ir(ppy)$_3$–Ir(ppy)$_3$ exciton interactions.[68,73] In neat films of fac-Ir(ppy)$_3$ critical current densities for quenching mechanisms like triplet–triplet annihilation are reported to be in the range I_d = 500–1400 mA cm^{-2}.[74,75] However, depending on the device structure, a decrease of EQE in neat films of fac-Ir(ppy)$_3$ can already be observed at current densities of I_d ≈ 300 mA cm^{-2}.[76] In LECs such quenching effects have also been studied in a few cases apart from the above-mentioned deactivation due to ligand loss and the formation of aqua complexes. The cationic iridium(III) complex [Ir(ppy)$_2$-(pzpy)]PF$_6$ [pzpy: 2-(1H-pyrazol-1-yl)pyridine] was tested in a LEC. The doping of this complex into a PMMA film (5 w/w%) increases its luminescence quantum yield (Φ = 23 → 61%) and lifetime (τ = 1.6 → 3.3 µs). However, luminescence quantum yield and lifetime drop dramatically when going from the doped (5 w/w % in PMMA) to the neat film (Φ = 3%, τ = 0.2 µs), which is attributed to the efficient excited state quenching in the neat film.[77] Quenching effects in LECs also depend on the thickness of the (neat) emitting layer. The EQE of a LEC with [Ru(bpy)$_3$]$(PF_6)_2$ decreases monotonically from 1% for a 192 nm thick complex layer to less than 0.01% for a 46 nm thick layer. The quenching is believed to occur by triplet–triplet annihilation and higher charge carrier densities near the electrode surfaces.[78–80] Self-quenching can be avoided by using sterically demanding substituents.[81,82] As a result of the high local concentration (neat or 80 w/w%), high current densities (up to 518 mA cm^{-2}), and high solution luminescence lifetimes (up to 841 ns), saturation and quenching effects might also be present in our LECs. Indeed, dilution with

PMMA has a positive effect on the EQE. In LECs with [**2**]$(PF_6)_2$ and [**3**]$(PF_6)_2$, the EQE is increased by a factor of two by using PMMA.[20,83] The maximum values of the EQE are obtained after 1–15 min. In LECs with PMMA of [**2**]$(PF_6)_2$ and [**3**]$(PF_6)_2$, the maximum EQE is reached after only one minute, which is attributed to the fast ion migration and rapid device degradation due to the high applied voltages of 5–6 V.[6]

Conclusions

Heteroleptic bis(tridentate) ruthenium(II) complexes [**1**]$(PF_6)_2$–[**3**]$(PF_6)_2$ (Figure 1) were used as emitters in LECs with a ITO/PEDOT:PSS/ruthenium(II) complex/Ag device structure. Red to NIR light emission was observed in the solid-state devices (λ_{em} = 722–755 nm; CIE: x = 0.709–0.731, y = 0.291–0.269). To the best of our knowledge, these are the lowest emission energies for LECs containing bis(tridentate) ruthenium(II) complexes. The low-energy emission is favored by the pronounced push-pull character of the complexes, which results in a small HOMO–LUMO gap. PMMA as additive (20% w/w) in the ruthenium complex layer requires higher driving voltages but yields higher external quantum efficiencies. Future perspectives include the steric protection of the ruthenium core by bulkier ligands to prevent a change in the coordination sphere by ligand substitution and self-quenching as well as the usage of other counterions to investigate their effect on the LEC performance.

Experimental Section

General Procedures: Complexes [**1**]$(PF_6)_2$–[**3**]$(PF_6)_2$ were prepared as described previously.[35,36,46,47] Before spin-coating, the complexes were further purified by reversed phase HPLC with a JASCO semipreparative HPLC system with a Reprosil C$_{18}$ column (5 µm) by using CH$_3$CN/water (96:4, v/v) as an eluent (10 mL min^{-1}) and UV/Vis detection at 502–539 nm. Patterned ITO glass substrates, which were cleaned in an ultrasonic bath, sequentially with acetone, isopropyl alcohol, and deionized water, were treated with UV/O$_3$ for 10 min before spin-coating. PEDOT:PSS (1:6 weight%, Al 4083; suspension in water; 1.3–1.7% solid content) was filtered (HP, 0.45 µm) and spin-coated (4000 rpm, 30 s, 4 s acceleration) onto the ITO substrate. After drying (1 h, 120 °C under reduced pressure), the substrate was transferred into an argon atmosphere. Ruthenium complexes (10 mg mL^{-1}) and PMMA (0 or 2 mg mL^{-1}, M$_W$ 120000) were dissolved in acetonitrile in an argon atmosphere and spin-coated onto the PEDOT:PSS layer (1000 rpm, 20 s, no acceleration). Silver electrodes were vapor-deposited on the substrates under a pressure of 3 × 10^{-6} Torr. The current–voltage characteristics were measured by using a source measurement unit (Keithley 236). The luminance and efficiencies were calculated from photocurrent measurement data obtained with a calibrated Si photodiode (Hamamatsu S5227–1010BQ). Electroluminescence spectra of the devices were obtained by an ICCD camera through an ARC 275 monochromator. AFM measurements were conducted in intermittent contact mode with two different instruments: A Veeco Dimension AFM was used for the measurement of the total height of the PEDOT:PSS and the

emitting layers and a XE-100 AFM was used to measure the thickness of the PEDOT:PSS layer. The spin-coated PEDOT:PSS and PEDOT:PSS-ruthenium complex layers were scratched with a razor, and the thickness of the layers was determined by the measured height differences.

DFT Studies: The DFT calculations were carried out with the *Gaussian 09*/DFT[84] series of programs. The LANL2DZ basis set[84] was used in the B3LYP formulation of DFT. No symmetry constraints were imposed on the molecules. The presence of energy minima was checked by analytical frequency calculations. The integral-equation-formalism polarizable continuum model (IEFPCM, CH_3CN) was employed for solvent modeling in all calculations. All calculations were performed without explicit counterions and solvent molecules.

Supporting Information (see footnote on the first page of this article): AFM images of scratched PEDOT:PSS/ruthenium complex:PMMA layers; emission spectra of [**1**](PF$_6$)$_2$ and [**3**](PF$_6$)$_2$ in solution and in LECs; current density vs. EQE intensity curves of the LECs; human eye response curve and emission spectra of [**1**](PF$_6$)$_2$–[**3**](PF$_6$)$_2$ in LECs.

Acknowledgments

[1] H. Xiang, J. Cheng, X. Ma, X. Zhou, J. J. Chruma, *Chem. Soc. Rev.* **2013**, *42*, 6128–6185.

[2] R. D. Costa, E. Ortí, H. J. Bolink, F. Monti, G. Accorsi, N. Armaroli, *Angew. Chem.* **2012**, *124*, 8300–8334; *Angew. Chem. Int. Ed.* **2012**, *51*, 8178–8211.

[3] R. D. Costa, E. Ortí, H. J. Bolink, *Pure Appl. Chem.* **2011**, *83*, 2115–2128.

[4] J. Slinker, D. Bernards, P. L. Houston, H. D. Abruña, S. Bernhard, G. G. Malliaras, *Chem. Commun.* **2003**, *19*, 2392–2399.

[5] E. Holder, B. M. W. Langeveld, U. S. Schubert, *Adv. Mater.* **2005**, *17*, 1109–1121.

[6] J. D. Slinker, J. Rivnay, J. S. Moskowitz, J. B. Parker, S. Bernhard, H. D. Abruña, G. G. Malliaras, *J. Mater. Chem.* **2007**, *17*, 2976–2988.

[7] Q. Pei, G. Yu, C. Zhang, Y. Yang, A. J. Heeger, *Science* **1995**, *269*, 1086–1088.

[8] Q. Pei, Y. Yang, G. Yu, C. Zhang, A. J. Heeger, *J. Am. Chem. Soc.* **1996**, *118*, 3922–3929.

[9] A. P. Monkman, *ISRN Mater. Sci.* **2013**, DOI: 10.1155/2013/670130.

[10] J. Wang, A. Chepelianskii, F. Gao, N. C. Greenham, *Nat. Commun.* **2012**, *3*, DOI: 10.1038/ncomms2194.

[11] A. Köhler, H. Bässler, *Mater. Sci. Eng.* **2009**, *R66*, 71–109.

[12] H. Yersin, *Highly Efficient OLEDs with Phosphorescent Materials*, Wiley-VCH, Weinheim, Germany, **2008**.

[13] J.-K. Lee, D. S. Yoo, E. S. Handy, M. F. Rubner, *Appl. Phys. Lett.* **1996**, *69*, 1686–1688.

[14] S. Campagna, F. Puntoriero, F. Nastasi, G. Bergamini, V. Balzani, *Top. Curr. Chem.* **2007**, *280*, 117–214.

[15] J. R. Lakowicz, *Principles of Fluorescence Spectroscopy*, Springer, New York, **2006**.

[16] A. Juris, V. Balzani, F. Barigelletti, S. Campagna, P. Belser, A. von Zelewsky, *Coord. Chem. Rev.* **1988**, *84*, 85–277.

[17] C.-Y. Liu, A. J. Bard, *Appl. Phys. Lett.* **2005**, *87*, 061110.

[18] H. Rudmann, S. Shimada, M. F. Rubner, *J. Am. Chem. Soc.* **2002**, *124*, 4918–4921.

[19] S. Xun, J. Zhang, X. Li, D. Ma, Z. Y. Wang, *Synth. Met.* **2008**, *158*, 484–488.

[20] H. Rudmann, M. F. Rubner, *J. Appl. Phys.* **2001**, *90*, 4338–4345.

[21] C. Fu, M. Wenzel, E. Treutlein, K. Harms, E. Meggers, *Inorg. Chem.* **2012**, *51*, 10004–10011.

[22] E. Meggers, *Chem. Eur. J.* **2010**, *16*, 752–758.

[23] M. Maestri, N. Armaroli, V. Balzani, E. C. Constable, A. M. W. Cargill Thompson, *Inorg. Chem.* **1995**, *34*, 2759–2767.

[24] R. Hogg, R. G. Wilkins, *J. Chem. Soc.* **1962**, 341–350.

[25] R. H. Holyer, C. D. Hubbard, S. F. A. Kettle, R. G. Wilkins, *Inorg. Chem.* **1966**, *5*, 622–625.

[26] A. Reynald, E. Palomares, *Eur. J. Inorg. Chem.* **2011**, *29*, 4509–4526.

[27] C.-W. Hsu, S.-T. Ho, K.-L. Wu, Y. Chi, S.-H. Liu, P.-T. Chou, *Energy Environ. Sci.* **2012**, *5*, 7549–7554.

[28] J.-F. Yin, M. Velayudham, D. Bhattacharya, H.-C. Lin, K.-L. Lu, *Coord. Chem. Rev.* **2012**, *256*, 3008–3035.

[29] B. Schulze, D. Escudero, C. Friebe, R. Siebert, H. Görls, S. Sinn, M. Thomas, S. Mai, J. Popp, B. Dietzek, L. González, U. S. Schubert, *Chem. Eur. J.* **2012**, *18*, 4010–4025.

[30] J. D. Slinker, J.-S. Kim, S. Flores-Torres, J. H. Delcamp, H. D. Abruña, R. H. Friend, G. G. Malliaras, *J. Mater. Chem.* **2007**, *17*, 76–81.

[31] L. J. Soltzberg, J. D. Slinker, S. Flores-Torres, D. A. Bernards, G. G. Malliaras, H. D. Abruña, J.-S. Kim, R. H. Friend, M. D. Kaplan, V. Goldberg, *J. Am. Chem. Soc.* **2006**, *128*, 7761–7764.

[32] G. Kalyuzhny, M. Buda, J. McNeill, P. Barbara, A. J. Bard, *J. Am. Chem. Soc.* **2003**, *125*, 6272–6283.

[33] J.-P. Sauvage, J.-P. Collin, J.-C. Chambron, S. Guillerez, C. Coudret, *Chem. Rev.* **1994**, *94*, 993–1019.

[34] Y. Liu, R. Hammitt, D. A. Lutterman, R. P. Thummel, C. Turro, *Inorg. Chem.* **2007**, *46*, 6011–6021.

[35] K. Heinze, K. Hempel, M. Beckmann, *Eur. J. Inorg. Chem.* **2006**, *10*, 2040–2050.

[36] K. Heinze, K. Hempel, S. Tschierlei, M. Schmitt, J. Popp, S. Rau, *Eur. J. Inorg. Chem.* **2009**, *21*, 3119–3126.

[37] K. Heinze, K. Hempel, A. Breivogel, *Z. Anorg. Allg. Chem.* **2009**, *635*, 2541–2549.

[38] K. Lashgari, M. Kritikos, R. Norrestam, T. Norrby, *Acta Crystallogr., Sect. C* **1999**, *55*, 64–67.

[39] M. Abrahamsson, M. Jäger, T. Österman, L. Eriksson, P. Persson, H.-C. Becker, O. Johansson, L. Hammarström, *J. Am. Chem. Soc.* **2006**, *128*, 12616–12617.

[40] G. A. Parada, L. A. Fredin, M.-P. Santoni, M. Jäger, R. Lomoth, L. Hammarström, O. Johansson, P. Persson, S. Ott, *Inorg. Chem.* **2013**, *52*, 5128–5137.

[41] M. Abrahamsson, M. Jäger, R. J. Kumar, T. Österman, P. Persson, H.-C. Becker, O. Johansson, L. Hammarström, *J. Am. Chem. Soc.* **2008**, *130*, 15533–15542.

[42] F. Schramm, V. Meded, H. Fliegl, K. Fink, O. Fuhr, Z. Qu, W. Klopper, S. Finn, T. E. Keyes, M. Ruben, *Inorg. Chem.* **2009**, *48*, 5677–5684.

[43] W. Y. Ng, X. Gong, W. K. Chan, *Chem. Mater.* **1999**, *11*, 1165–1170.

[44] H. J. Bolink, L. Cappelli, E. Coronado, P. Gaviña, *Inorg. Chem.* **2005**, *44*, 5966–5968.

[45] H. J. Bolink, E. Coronado, R. D. Costa, P. Gaviña, E. Ortí, S. Tatay, *Inorg. Chem.* **2009**, *48*, 3907–3909.

[46] A. Breivogel, M. Meister, C. Förster, F. Laquai, K. Heinze, *Chem. Eur. J.* **2013**, *19*, 13745–13760.

[47] A. Breivogel, C. Förster, K. Heinze, *Inorg. Chem.* **2010**, *49*, 7052–7056.

[48] A. Breivogel, K. Hempel, K. Heinze, *Inorg. Chim. Acta* **2011**, *374*, 152–162.

[49] H. Komatsu, K. Yoshihara, H. Yamada, Y. Kimura, A. Son, S.-i. Nishimoto, K. Tanabe, *Chem. Eur. J.* **2013**, *19*, 1971–1977.

[50] M. R. Gill, J. A. Thomas, *Chem. Soc. Rev.* **2012**, *41*, 3179–3192.

[51] P. Ceroni, *Chem. Eur. J.* **2011**, *17*, 9560–9564.

[52] T. N. Singh-Rachford, F. N. Castellano, *Coord. Chem. Rev.* **2010**, *254*, 2560–2573.

[53] W. Wu, S. Ji, W. Wu, J. Shao, H. Guo, T. D. James, J. Zhao, *Chem. Eur. J.* **2012**, *18*, 4953–4964.

[54] P. Hanczyc, B. Norden, M. Samoc, *Dalton Trans.* **2012**, *41*, 3123–3125.

[55] M. D. Ward, *Coord. Chem. Rev.* **2007**, *251*, 1663–1677.

[56] S. V. Eliseeva, J.-C. G. Bünzli, *Chem. Soc. Rev.* **2010**, *39*, 189–227.

[57] J. C. G. Bünzli, S. V. Eliseeva, *J. Rare Earths* **2010**, *28*, 824–842.

[58] T. J. Meyer, *Pure Appl. Chem.* **1986**, *58*, 1193–1206.

[59] J. V. Caspar, T. J. Meyer, *J. Am. Chem. Soc.* **1983**, *105*, 5583–5590.

[60] J. V. Caspar, T. J. Meyer, *J. Phys. Chem.* **1983**, *87*, 952–957.

[61] E(vacuum) /eV = –4.68 – E(SCE) /V = –5.08 – E(Fc/Fc$^+$) /V.

[62] F. Bolletta, S. Bonafede, *Pure Appl. Chem.* **1986**, *58*, 1229–1232.

[63] F. Xu, J.-Y. Kwon, J.-H. Kim, H. U. Kim, J. M. Lim, H. Cho, C. Lee, J. Lee, J.-I. Lee, D.-H. Hwang, *Synth. Met.* **2012**, *162*, 1421–1428.

[64] H. J. Bolink, L. Cappelli, E. Coronado, M. Grätzel, Md. K. Nazeeruddin, *J. Am. Chem. Soc.* **2006**, *128*, 46–47.

[65] International Commission on Illumination (CIE), 1931.

[66] P. Toivanen, J. Hovila, P. Kärhä, E. Ikonen, *Metrologia* **2000**, *37*, 527–530.

[67] P. Toivanen, P. Kärhä, F. Manoochehri, E. Ikonen, *Metrologia* **2000**, *37*, 131–140.

[68] H. Yersin, A. F. Rausch, R. Czerwieniec, T. Hofbeck, T. Fischer, *Coord. Chem. Rev.* **2011**, *255*, 2622–2652.

[69] N. C. Giebink, S. R. Forrest, *Phys. Rev. B* **2008**, *77*, 235215.

[70] T. Hofbeck, H. Yersin, *Inorg. Chem.* **2010**, *49*, 9290–9299.

[71] M. A. Baldo, C. Adachi, S. R. Forrest, *Phys. Rev. B* **2000**, *62*, 10967–10977.

[72] M. A. Baldo, M. E. Thompson, S. R. Forrest, *Pure Appl. Chem.* **1999**, *71*, 2095–2106.

[73] C. Adachi, M. A. Baldo, S. R. Forrest, M. E. Thompson, *Appl. Phys. Lett.* **2000**, *77*, 904–906.

[74] J. Kalinowski, J. Mżyk, F. Meinardi, R. Tubino, M. Cocchi, D. Virgili, *J. Appl. Phys.* **2005**, *98*, 063532.

[75] J. Kalinowski, W. Stampor, J. Szmytkowski, D. Virgili, M. Cocchi, V. Fattori, C. Sabatini, *Phys. Rev. B* **2006**, *74*, 085316.

[76] M. A. Baldo, S. Lamansky, P. E. Burrows, M. E. Thompson, S. R. Forrest, *Appl. Phys. Lett.* **1999**, *75*, 4–6.

[77] L. He, L. Duan, J. Qiao, R. Wang, P. Wei, L. Wang, Y. Qiu, *Adv. Funct. Mater.* **2008**, *18*, 2123–2131.

[78] K. W. Lee, J. D. Slinker, A. A. Gorodetsky, S. Flores-Torres, H. D. Abruña, P. L. Houston, G. G. Malliaras, *Phys. Chem. Chem. Phys.* **2003**, *5*, 2706–2709.

[79] S. Bernhard, X. Gao, G. G. Malliaras, H. D. Abruña, *Adv. Mater.* **2002**, *14*, 433–436.

[80] N. R. Armstrong, R. M. Wightman, E. M. Gross, *Annu. Rev. Phys. Chem.* **2001**, *52*, 391–422.

[81] P. Dreyse, B. Loeb, M. Soto-Arriaza, D. Tordera, E. Ortí, J. J. Serrano-Pérez, H. J. Bolink, *Dalton Trans.* **2013**, *42*, 15502–15513.

[82] S. Bernhard, J. A. Barron, P. L. Houston, H. D. Abruña, J. L. Ruglovksy, X. Gao, G. G. Malliaras, *J. Am. Chem. Soc.* **2002**, *124*, 13624–13628.

[83] D. W. Thompson, C. N. Fleming, B. D. Myron, T. J. Meyer, *J. Phys. Chem. B* **2007**, *111*, 6930–6941.

[84] M. J. Frisch, G. W. Trucks, H. B. Schlegel, G. E. Scuseria, M. A. Robb, J. R. Cheeseman, G. Scalmani, V. Barone, B. Mennucci, G. A. Petersson, H. Nakatsuji, M. Caricato, X. Li, H. P. Hratchian, A. F. Izmaylov, J. Bloino, G. Zheng, J. L. Sonnenberg, M. Hada, M. Ehara, K. Toyota, R. Fukuda, J. Hasegawa, M. Ishida, T. Nakajima, Y. Honda, O. Kitao, H. Nakai, T. Vreven, J. A. Montgomery Jr., J. E. Peralta, F. Ogliaro, M. Bearpark, J. J. Heyd, E. Brothers, K. N. Kudin, V. N. Staroverov, R. Kobayashi, J. Normand, K. Raghavachari, A. Rendell, J. C. Burant, S. S. Iyengar, J. Tomasi, M. Cossi, N. Rega, J. M. Millam, M. Klene, J. E. Knox, J. B. Cross, V. Bakken, C. Adamo, J. Jaramillo, R. Gomperts, R. E. Stratmann, O. Yazyev, A. J. Austin, R. Cammi, C. Pomelli, J. W. Ochterski, R. L. Martin, K. Morokuma, V. G. Zakrzewski, G. A. Voth, P. Salvador, J. J. Dannenberg, S. Dapprich, A. D. Daniels, O. Farkas, J. B. Foresman, J. V. Ortiz, J. Cioslowski, D. J. Fox *Gaussian 09*, revision A.02, Gaussian, Inc., Wallingford CT, **2009**.